Superconducting transition-edge-microcalorimeter x-ray spectrometer with 2 eV energy resolution at 1.5 keV*

D. A. Wollman[a, **], S. W. Nam[a], Dale E. Newbury[b], G. C. Hilton[a], K. D. Irwin[a], N. F. Bergren[a], S. Deiker[a], D. A. Rudman[a], John M. Martinis[a]

[a] *National Institute of Standards and Technology (NIST), Boulder, CO 80303, USA*
[b] *National Institute of Standards and Technology (NIST), Gaithersburg, MD 20899, USA*

Received 8 August 1999

Abstract

We describe the operation and performance of a prototype microcalorimeter "energy-dispersive" (non-dispersive) x-ray spectrometer (μcal EDS) developed at NIST for use in x-ray microanalysis and x-ray astronomy. The low-energy microcalorimeter detector, consisting of an Al-Ag bilayer superconducting transition-edge sensor (TES) in thermal contact with a Bi x-ray absorber, is designed for operation in the energy range from 0 keV to 2 keV and is fabricated using a shadow-mask lithographic process. The TES microcalorimeter is cooled by a compact adiabatic demagnetization refrigerator and is mounted on a scanning electron microscope. This device achieves a best energy resolution of 2.0 eV ± 0.1 eV at 1.5 keV, as determined from the analysis of digitized x-ray spectra of a complex glass containing many elements.

PACS: 07.20.Me, 07.57.Kp, 07.85Fv, 07.85.Nc, 29.30.Kv, 81.70.Jb

Keywords: Microcalorimeter, Microcalorimeter EDS, Energy-dispersive spectrometer, X-ray microanalysis, Transition-edge sensor, Cryogenic device, Energy resolution, X-ray detector, Non-dispersive detector

1. Introduction

We have recently developed a superconducting transition-edge microcalorimeter "energy-dispersive" (non-dispersive) spectrometer [1] (μcal EDS) with high energy resolution for use in x-ray microanalysis. X-ray microanalysis is a sensitive, nondestructive analytical technique that provides spatially resolved qualitative and quantitative microchemical analysis. Typically, a beam of finely focused electron or x-rays is used to excite x rays in a small region of a sample. The emitted x rays are then analyzed using a commercially available wavelength-dispersive spectrometer (WDS) or semiconductor-based EDS to obtain an x-ray spectrum. Comparing the integrated characteristic x-ray intensities produced by the sample and by elemental standards yields qualitative and quantitative compositional information on a length scale of micrometers or less.

Unfortunately, neither semiconductor EDS nor WDS fully satisfy the microanalysis requirements facing many technology-intensive industries. In a semiconductor EDS detector, x rays are absorbed in a voltage-biased intrinsic semiconductor to create electron-hole pairs, which separate under the applied electric field to yield a collected charge proportional to the x-ray energy. Semiconductor EDS is used in over 90% of installed x-ray microanalysis systems because it is

** Corresponding author. Tel.: 303-497-7457; fax: 303-497-3042.
E-mail address: david.wollman@nist.gov

easy to use, inexpensive to operate, and offers both rapid qualitative evaluation of chemical composition and accurate quantitative analysis. However, it is limited by an energy resolution on the order of 100 eV, which is insufficient to resolve many important overlapping x-ray peaks in materials of industrial interest, such as the Si Kα and W Mα peak overlap in WSi_2. In contrast, WDS uses Bragg reflection from curved diffracting crystals to achieve the excellent resolution (typically 2 eV to 20 eV) needed to resolve most peak overlaps. However, qualitative WDS analysis is severely limited by the long time needed to serially scan over the entire energy range using multiple diffraction crystals.

There is a need for a new generation of x-ray spectrometer for x-ray microanalysis that combines the excellent energy resolution of WDS with the ease of use and the parallel energy detection capability of energy-dispersive semiconductor EDS. X-ray spectrometers based on several cryogenic detectors have been proposed to fill this need: candidate detectors include transition-edge sensor (TES) microcalorimeters [1], semiconductor thermistor microcalorimeters [2-4], and superconducting tunnel junction (STJ) detectors [5]. In this paper, we briefly describe the operation and current performance of the prototype superconducting transition-edge microcalorimeter EDS (μcal EDS) system [1, 6] developed at NIST.

2. TES Microcalorimeter Operation and Instrumentation

The transition-edge microcalorimeter developed at NIST uses a TES thermometer, which is a superconducting film biased in temperature within its narrow resistive transition from the normal to the superconducting state. The TES is biased with a voltage V, and the current flowing through the film is measured with a low-noise superconducting quantum interference device (SQUID) amplifier. The heat bath is then cooled to well below the transition temperature of the film, chosen for the device reported here to be 100 mK. As the TES cools, its resistance R drops and the Joule heating (V^2/R) in the film increases. A stable equilibrium is established when the resistance is reduced to the point where the Joule heating equals the heat flowing to the heat bath. The TES thus self-regulates in temperature within its transition, an effect referred to as negative electrothermal feedback [7].

When an x ray deposits its energy in the absorber, the temperature and resistance of the TES increase, leading to a decrease in the current and thus descreased dissipation of Joule power in the TES, while the heat flowing to the heat bath remains approximately constant. Thus, the x-ray energy is primarily removed by a reduction in Joule heating, which can lead to a thermal response time more than a hundred times faster [7] than the natural relaxation time $t = C/G$, where C is the heat capacity and G is the thermal conductance between the TES and the lower temperature heat sink. This faster time constant significantly increases the output count rate of TES microcalorimeters (to ~500 s^{-1}, at present), making these microcalorimeters attractive for many real-world microanalysis applications.

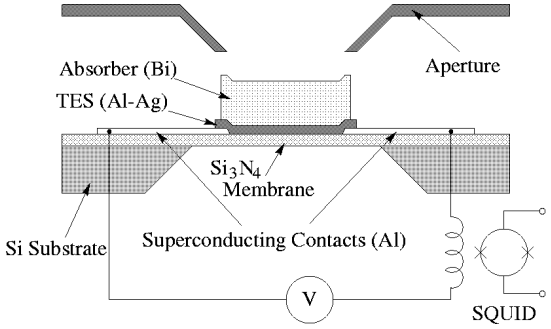

Fig. 1. Cross-sectional view of the TES microcalorimeter. An x ray passes through an aperture and is absorbed in the Bi film. The resulting thermal energy pulse raises the temperature of the TES, causing an increase in resistance of the TES, and a pulse of decreased current at the SQUID input.

Figure 1 shows a cross-sectional view of a TES microcalorimeter, including the physical layout and the external electrical connections. Using electron-beam evaporation through shadow masks, the TES, Bi absorber, and electrical contacts are deposited on a 0.25 μm thick freely suspended silicon nitride membrane supported by a micromachined silicon substrate. The thin membrane reduces the thermal conductance from the detector to the bath, prevents the loss of absorbed x-ray energy via high-energy phonons escaping into the substrate, and eliminates x-ray absorption in the substrate. Additionally, the

electrical contacts to the TES are made with superconducting aluminum lines, which have very small thermal conductivity. The TES itself is 400 μm by 400 μm in lateral area and consists of a ~300 nm thick Ag/Al bilayer. Proximity coupling between the normal metal Ag and the superconducting Al provides sharp and reproducible superconducting transitions at temperatures in the range 50 mK to 1 K. The thicknesses of the two metals were chosen to obtain a transition temperature of 100 mK for the device reported here. A 1.5 μm thick Bi film deposited on top of the TES bilayer is used as the x-ray absorber. A 350 μm diameter circular Pt aperture collimates incoming x rays so that they are incident only on the absorber.

The low impedance of the TES (R_n ~ 30 mΩ for the device reported here) allows efficient coupling to low-noise, low-power SQUID amplifiers. Because the detector's electrical bandwidth is limited by the L/R time constant of the SQUID input circuit (L is the sum of the stray and SQUID input inductances, and R is the sum of the TES dynamic resistance and the bias resistance), improved speed and stability are obtained by mounting a first-stage SQUID at 0.1 K close to the detector chip, thus minimizing stray inductance. The output of this SQUID is amplified by a series-array SQUID operating at 4 K. The large output voltage (5 mV) and high output impedance (100 Ω) of the series-array SQUID allows the use of simple room temperature amplifiers for read out. At this stage, signal pulses resulting from discrete x-ray photon events are filtered and digitized for off-line analysis or shaped for real-time peak height analysis using a commercially available EDS multichannel analyzer. In addition, for real-time acquisition, pulse pileup rejection circuitry is used to veto x-ray pulses that are coincident in time.

For μcal EDS to be practical and useful to industry, a convenient and simple refrigeration system is required to reach operating temperatures of less than 100 mK. The refrigerator must be compact enough to be mounted on an scanning electron microscope (SEM), have low vibration, and be very simple to operate. To satisfy these requirements, we have constructed a compact adiabatic demagnetization refrigerator [8] (ADR), installed in a commercial two-cryogen (liquid helium and liquid nitrogen) cryostat to provide cooling from the liquid helium reservoir at 4 K to a base temperature of 45 mK. A typical detector stage operating temperature of 70 mK can be held for over 12 hours, after which the ADR requires a magnetic "recharge" cycle that takes less than 45 minutes to complete.

To increase the fraction of x rays collected from the sample, the TES microcalorimeter is placed at the end of a long Cu rod cooled by the ADR and surrounded by heat and vacuum shields that protrude from the cryostat and extend into the SEM. A commercial vacuum-tight x-ray window placed at the end of the snout permits x-ray illumination of the detector. Within the snout, two free-standing Al-coated polymer membranes at 4 K and a third at 70 mK are positioned between the x-ray window and the detector, reducing the infrared heat load on the detector. This arrangement allows us to place the detector less than 30 mm from the SEM sample stage.

Although our TES microcalorimeter has a small collection area (0.16 mm^2), we have dramatically increased its effective detector area using polycapillary x-ray optics [1]. These optics utilize high-efficiency grazing-angle x-ray reflections to deflect x rays over a wide angle. A polycapillary optic consisting of tens of thousands of fused glass capillaries collects x rays from a point x-ray source and focuses the x rays onto the small area absorber of our detector, as shown in Fig 2. This

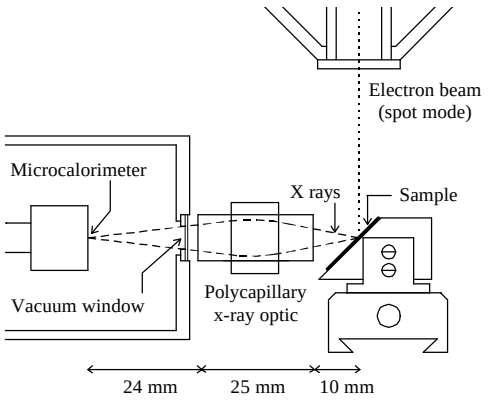

Fig. 2. Diagram (approximately to scale) of microcalorimeter, polycapillary x-ray optic, and sample inside the SEM chamber, adapted from Ref. 1. By mechanically positioning the optic, the input and output focal spots of the optic are aligned with the sample and the microcalorimeter. For clarity, translation stages, heat shields and infrared-blocking Al filters are not shown.

technique increases the effective area of the microcalorimeter to ~5 mm^2 (relative to an effective sample-detector distance of 25 mm) over a broad range of x-ray energies (200 eV to 10 keV).

3. Current performance of μcal EDS

To be of practical value, μcal EDS must show significant performance increases over currently available techniques. The current performance of μcal EDS approaches that of high-resolution semiconductor EDS in terms of solid angle (~0.008 sr with a polycapillary optic x-ray lens, compared to 0.025 sr) and maximum count rate (~500 s^{-1} compared to 3000 s^{-1}), while providing improved energy resolution, comparable to that of WDS. The excellent energy resolution of our low-energy μcal EDS (~4 eV FWHM for real-time analog processing over the energy range 0 keV to ~2 keV) allows straightforward identification of closely spaced x-ray peaks in complicated spectra, including overlapping peaks in important materials (such as TiN and WSi_2) which cannot be resolved by semiconductor EDS. The ability to resolve peak overlaps using this detector is clearly observed in Fig. 3, in which we show an x-ray

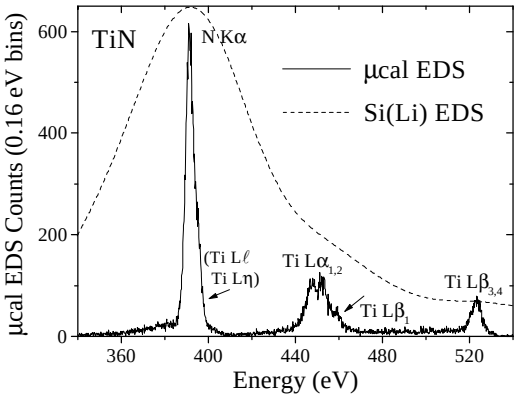

Fig. 3. Microcalorimeter EDS spectrum (μcal EDS, solid line) of TiN, acquired in real time using analog pulse processing under the following conditions: 3 keV beam energy, 1.44 nA beam current, 520 s^{-1} input count rate, 320 s^{-1} output count rate, 39% dead time, 500 s live time, and a 45° x-ray takeoff angle. Typical 1/e detector pulse falltimes for all data reported here are approximately 120 μs. Also shown for comparison is a semiconductor EDS spectrum (Si(Li) EDS, dashed line) of TiN.

spectrum of TiN acquired in real time with our μcal EDS mounted on a SEM. The impressive increase in resolution over that of semiconductor EDS, coupled with reasonable output count rates and solid angle, show the usefulness of microcalorimeter EDS for x-ray microanalysis.

In Fig. 4, we show the μcal EDS spectrum of a complex glass (K3670) synthesized at NIST and designed to have many evenly spaced x-ray lines to serve as an energy-calibration target. These lines allow the energy nonlinearity of the detector to be easily characterized and modeled with a

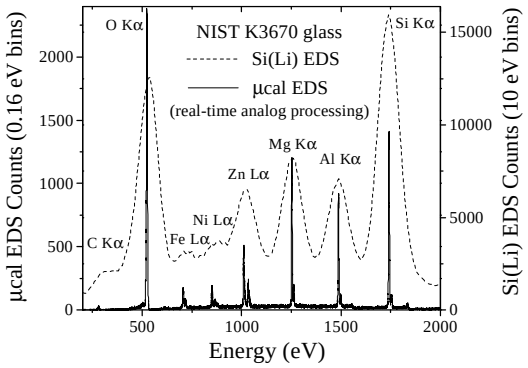

Fig. 4. Microcalorimeter EDS (μcal EDS, solid line) spectrum of the multielement NIST K3670 glass, acquired in real time using analog pulse processing under the following conditions: 3 keV beam energy, 0.53 nA beam current, 320 s^{-1} input count rate, 230 s^{-1} output count rate, 28% dead time, 1500 s live time, and a 45° x-ray takeoff angle. Also shown for comparison is a semiconductor EDS (Si(Li) EDS, dashed line) spectrum of the same glass, acquired under the following conditions: 5 keV beam energy, 5 nA beam current, 2300 s^{-1} input count rate, 1600 s^{-1} output count rate, 30% dead time, 500 s live time, and a 40° x-ray takeoff angle.

polynomial fit. The fit is then used in a software-based real-time linearity correction routine, which operates ahead of the histogram binning of the incoming photon counts. The spectra presented in Figs. 3 and 4 were both acquired using this real-time linearity correction.

X rays from this energy-calibration glass were also collected as filtered and digitized x-ray pulses, which were then analyzed using optimal filtering to produce a spectrum. The Al-Kα portion of this spectrum is shown in Fig. 5. Also shown in Fig. 5 is the weighted-least-squares fit of the Al $K\alpha_{1,2}$ and Al $K\alpha'_{3,4,5,6}$ satellite x rays to a convolution of the theoretical line profiles and a

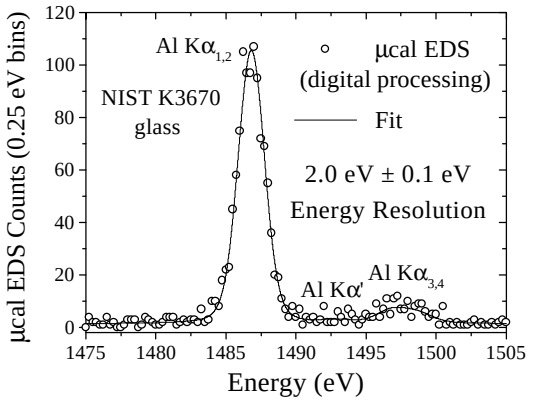

Fig. 5. The Al-Kα region of a digitized μcal EDS spectrum of the multielement NIST K3670 glass (with Al in an Al oxide chemical state, assumed to be Al_2O_3), obtained from the analysis of digitized and optimally filtered x-ray pulses. This spectrum was acquired using a beam energy of 5.0 keV and corrected for detector energy nonlinearity. Also shown is the weighted least-squares fit of the Al $K\alpha_{1,2}$ and Al $K\alpha'_{3,4,5,6}$ satellite x rays to a convolution of the theoretical line profiles and a Gaussian instrument response, yielding an energy resolution of 2.0 eV ± 0.1 eV at 1.5 keV.

Gaussian instrument response, yielding an energy resolution of 2.0 eV ± 0.1 eV at 1.5 keV. For this fit, a mostly consistent set of Al-Kα x-ray line positions, relative intensities, and Lorentzian natural line widths (appropriate for Al in Al_2O_3, 5 keV beam energy) was obtained by cross-correlating results from the literature [9-12]:
Al $K\alpha_1$ (1486.94 eV, 1.0 relative intensity, 0.43 eV line width), Al $K\alpha_2$ (1486.52 eV, 0.5 relative intensity, 0.43 eV line width), Al Kα' (1492.94 eV, 0.033 relative intensity, 1.34 eV line width), Al $K\alpha_3$ (1496.85 eV, 0.12 relative intensity, 0.96 eV line width), Al $K\alpha_4$ (1498.70 eV, 0.11 relative intensity, 1.25 eV line width), Al $K\alpha_5$ (1507.4 eV, 0.07 relative intensity, 1.5 eV line width), Al $K\alpha_6$ (1510.9 eV, 0.05 relative intensity, 0.9 eV line width). We performed a fit to the data using 5 free parameters ($K\alpha_1$ intensity, $K\alpha_1$ line energy, instrumental energy resolution, differential nonlinearity, and constant background), with other line profiles constrained as above.

In addition, we analyzed the glass spectrum to obtain the instrumental energy resolutions at the Mg-Kα and Si-Kα x-ray lines, which were found to be consistent with the reported resolution at the Al-Kα line; however, these results are not reported due to our inability to find measured line profiles appropriate for Mg and Si oxides in the literature.

4. Conclusion

We have developed a high-resolution μcal EDS based on superconducting transition-edge microcalorimeter x-ray detectors for use in x-ray microanalysis. With an energy resolution of 2 eV at 1.5 keV (digital processing), a count rate of ~500 s^{-1} (analog processing), and an effective collection area of ~5 mm^2 (using polycapillary x-ray optics), the prototype μcal EDS combines the favorable qualities of wavelength dispersive spectrometers (WDS) and semiconductor EDS. With commercialization (in progress) and further development, μcal EDS will help to meet the analytical requirements for x-ray microanalysis in the future.

References

[1] D. A. Wollman, K. D. Irwin, G. C. Hilton, L. L. Dulcie, D. E. Newbury, and J. M. Martinis, J. Microscopy, 188 (1997) 196.
[2] D. McCammon, W. Cui., M. Juda, P. Plucinsky, J. Zhang, R. L. Kelley, S. S. Holt, G. M. Madejski, S. H. Moseley, and A. E. Szymkowiak, Nucl. Phys. A 527 (1991) 821c.
[3] L. Lesyna, D. Di Marzio, S. Gottesman, and M. Kesselman, J. Low. Temp. Phys. 93 (1993) 779.
[4] E. Silver, M. LeGros, N. Madden, J. Beeman, and E. Haller, X-Ray Spectrom. 25 (1996) 115.
[5] M. Frank, L. J. Hiller, J. B. le Grand, C. A. Mears, S. E. Labov, M. A. Lindeman, H. Netel, and D. Chow, Rev. Sci. Instrum. 69 (1998) 25.
[6] D. A. Wollman *et al*., Characterization and Metrology for ULSI Technology: 1998 International Conference (1998) 799.
[7] K. D. Irwin, Appl. Phys. Lett. 66 (1995) 1998.
[8] C. Hagmann and P. Richards, Cryogenics 34 (1994) 221.
[9] D. W. Fisher and W. L. Baun, J. Appl. Phys. 36 (1965) 534; J. Utriainen *et al*., Z. Naturforsch 23a (1968) 1178.
[10] C. Klauber, Surface and Interface Analysis 20 (1993) 703; K. H. Richter, Surface and Interface Analysis 15 (1990) 705.
[11] J. Schweppe, R. D. Deslattes, T. Mooney, and C. J. Powell, J. Electron. Spectroscopy and Related Phenomena 67 (1994) 463.
[12] M. O. Krause and J. H. Oliver, J. Phys. Chem. Ref. Data 8 (1979) 329; M. O. Krause,

ibid., 307; S. T. Perkins, *et al*., (1991) Tables and graphs of atomic subshell and relaxation data derived from the LLNL Evaluated Atomic Data Library (EADL), Z=1-100. Lawrence Livermore National Laboratory, Livermore.